NOVEL SULFOGLYCOLIPID IG20 CAUSES NEUROPROTECTION BY ACTIVATING THE PHASE II ANTIOXIDANT RESPONSE IN RAT HIPPOCAMPAL SLICES

By

Eva Punzón[1,*], Fernanda García-Alvarado[1,2,*], Marcos Maroto[1,2,*], Cristina Fernández[1,2], Patrycja Michalska[1,2], Isabel García-Álvarez[4], Juan Alberto Arranz-Tagarro[1], Izaskun Buendia[1,2], Manuela G. López[1,2], Rafael León[1,3], Luis Gandía[1,2], Alfonso Fernández-Mayoralas[5] and Antonio G. García[1,2,3]

From

[1]Instituto Teófilo Hernando, [2]Departamento de Farmacología y Terapéutica, Facultad de Medicina, Universidad Autónoma de Madrid, C/ Arzobispo Morcillo, 4; 28029 Madrid, Spain,

[3]Servicio de Farmacología Clínica, Instituto de Investigación Sanitaria, Hospital Universitario de la Princesa, Universidad Autónoma de Madrid, c/ Diego de León, 62; 28006 Madrid, Spain

[4]Hospital Nacional de Parapléjicos, SESCAM, Finca La Peraleda s/n, 45071 Toledo, Spain;

[5]Instituto de Química Orgánica General, CSIC, Juan de la Cierva 3, 28006 Madrid, Spain;

*Equal contributors

Short title: Novel sulfoglycolipid IG20 causes neuroprotection

Correspondence: Dr. Antonio G. García
Instituto Teófilo Hernando
Departamento de Farmacología y Terapéutica
Facultad de Medicina
Universidad Autónoma de Madrid
c/ Arzobispo Morcillo, 4
28029 - Madrid
Email: agg@uam.es

Summary

Compound IG20 is a newly synthesised sulphated glycolipid that promotes neuritic outgrowth and myelinisation, at the time it causes the inhibition of glial proliferation and facilitates exocytosis in chromaffin cells. Here we have shown that IG20 at 0.3-10 μM afforded neuroprotection in rat hippocampal slices stressed with veratridine, glutamate or with oxygen plus glucose deprivation followed by reoxygenation (OGD/reox). Excess production of reactive oxygen species (ROS) elicited by glutamate or ODG/reox was prevented by IG20 that also restored the depressed tissue levels of GSH and ATP in hippocampal slices subjected to OGD/reox. Furthermore, the augmented iNOS expression produced upon OGD/reox exposure was also counteracted by IG20. Additionally, the IG20 elicited neuroprotection was prevented by the presence of inhibitors of the signalling pathways Jak2/STAT3, MEK/ERK1/2, and PI3K/Akt, consistent with the ability of the compound to increase the phosphorylation of Jak2, ERK1/2, and Akt. Thus, the activation of phase II response and the Nrf2/ARE pathway could explain the antioxidant and anti-inflammatory effects and the ensuing neuroprotective actions of IG20.

Keywords: Sulfoglycolipid IG20, neurotoxicity, neuroprotection, oxidative stress, neuronal excitability, hippocampal slices, hippocampal neurons

1.- Introduction

Sulfoglycolipid IG20 was designed and synthesised at our laboratory in the context of a programme to obtain new compounds aimed at promoting neuritogenesis and myelinisation, with a special focus to inhibit glial proliferation. This last property mainly focused the treatment of cerebral gliomas (Doncel-Perez et al., 2013; Fernandez-Mayoralas et al., 2003; Garcia-Alvarez et al., 2007). The synthetic strategy was inspired in the fact that in mammalian brain there are natural inhibitors of astroblasts and astrocytes division (Nieto-Sampedro, 1988; Nieto-Sampedro and Broderick, 1989); one such inhibitor is neurostatin, first found in the rat brain (Valle-Argos et al., 2010). Although neurostatin happened to be a very potent blocker of glial proliferation, its molecular complexity makes difficult its purification from brain tissue or its laboratory synthesis. Thus, the simple compound IG20 was synthesised and although with lesser potency, it shared with neurostatin its ability to inhibit gliomas growth (Garcia-Alvarez et al., 2007). Recently, IG20 was shown to inhibit astrocyte and microglia proliferation, the main cellular components of the glial scar, and promote axonal outgrowth and myelin production *in vitro* (Garcia-Alvarez et al., 2015). This compound has a structure very similar to sulfatides, a class of sulfated galactosylceramides that are synthesised mainly in brain oligodendrocytes and belong to the great family of sphingosine derived sphingolipids (Honke, 2013) (Fig.1).

From a drug therapy point of view, compounds like IG20 could have various potential clinical applications. For instance, sulfatides are known to play a relevant role in myelin stabilisation and function (Coetzee et al., 1996). In fact, KO mice for sulfatide synthesising enzyme develop thinner myelin sheets and progressive paralysis (Honke, 2013). Also, a recent study shows changes in sulfatide brain levels at early stages of Alzheimer´s disease (AD) (Cheng et al., 2013). Thus, the ability of IG20 to inhibit astrocyte and microglia proliferation indicates its potential therapeutic application to mitigate the neuroinflammatory component in the pathogenesis of AD and Parkinson´s disease (PD). Additionally, in promoting myelinisation, IG20-type compounds could find a clinical application in multiple sclerosis. Finally, IG20 could also be potentially useful in brain repair after a traumatic brain or spinal cord damage; in these conditions, the recruitment of inflammatory cells and astrocytes contribute to the formation of a glial scare that impede axonal growth and regeneration (Yiu and He, 2006) and IG20-like compounds could prevent the formation of the glial scare.

We have recently found that IG20 facilitates the exocytotic release of transmitter, apparently through the regulation of a voltage-dependent sodium channel current in bovine chromaffin cells (Crespo-Castrillo et al., 2015). This property may additionally contribute to the ability of IG20 to promote synaptic plasticity. Additionally, the inhibition of glial proliferation and augmentation of neuritogenesis could translate into a neuroprotective effect of IG20. We have explored here this hypothesis in acutely isolated rat hippocampal slices stressed with various neurotoxic stimuli. We have found that IG20 exhibited a clear neuroprotective effect that was associated to its ability to activate the phase II antioxidant response that includes among others, haemoxygenase-1 (HO-1) and the catalytic subunit of glutamate-cysteine ligase (GCLcat), the rate-limiting enzyme for glutathione (GSH) (Egea et al., 2015; Zhang et al., 2013).

2.- Material and methods

2.1.- Synthesis of compound IG20

IG20 was synthesized using a new procedure which involves a regioselective sulfation (Garcia-Alvarez et al., 2015). Briefly, oleyl *N*-acetylglucosaminide in anhydrous pyridine was treated with SO_3-pyridine complex (1.2 equiv) at 0 °C for 1.5 h and at room temperature for 2 h. The solvent was removed and the residue was dissolved in 2:1 MeOH-H_2O, neutralized with a 0.5 M KOH solution and concentrated. The residue was purified by silica gel column chromatography (CH_2Cl_2/MeOH, 4:1 to 2:1) to give IG20 as a white solid (81%).

2.2.- Preparation of hippocampal slices

All experiments were carried out in accordance with the code of ethics and guidelines established by European Community Directive (2010/63/EU) and Spanish legislation 1201/2005. All animals used in this study were provided by the local university's facilities where they were housed (EX 021-U). All efforts were made to minimise the number of animals and their suffering.

Experiments were performed in hippocampal slices prepared from brains of adult male Sprague-Dawley rats (*Rattus norvegicus;* 250-300 g weight). Rats were killed by decapitation under anaesthesia with sodium pentobarbital (60 mg/Kg i.p.). The brain was rapidly removed from the skull and placed into oxygenated ice-cold Krebs-bicarbonate dissection buffer containing (in mM): NaCl 120, KCl 2, $NaHCO_3$ 26, KH_2PO_4 1.18, $CaCl_2$ 0.5, glucose 11, sucrose 200 and $MgSO_4$ 10. Slices (300 µm thick) were prepared using a Mcllwain tissue chopper and separated in ice-cold dissection buffer. Then they were immediately transferred to a vial containing sucrose-free buffer of the following composition (in mM): NaCl 120, KCl 2, $NaHCO_3$ 26, KH_2PO_4 1.18, $CaCl_2$ 2, glucose 11 and $MgSO_4$ 1.19; it was bubbled with 95% O_2 and 5% CO_2 for 45 min at 34°C to recover from slicing trauma. After the stabilisation period, slices were bubbled during 30 min at 37°C in a control buffer containing (in mM): NaCl 120, KCl 2, $NaHCO_3$ 26, KH_2PO_4 1.18, $CaCl_2$ 2, glucose 11 and $MgSO_4$ 1.19.

2.3.- Cell Cultures

For the isolation and culture of hippocampal neurons, pregnant Sprague-Dawley rats were decapitated under anaesthesia with sodium pentobarbital (60 mg/Kg i.p.) and 18-day embryos were removed immediately by caesarean section. Hippocampi were dissected rapidly under a stereomicroscope and sterile conditions in ice-cold phosphate buffer solution (PBS) of the following composition (in mM): NaCl, 137; KCl, 2.7; NaH_2PO_4, 11.6; and KH_2PO_4 1.47 (pH 7.4, adjusted with NaOH). The tissue was digested with 0.5 mg/mL papain (Sigma-Aldrich. Madrid, Spain). The enzyme was dissolved in a Ca^{2+}- and Mg^{2+}-free PBS solution containing 1 mg/mL BSA and 10 mM glucose at 37°C for 20 min. The papain solution was replaced with 5 mL of Neurobasal medium (Gibco-Invitrogen; Barcelona, Spain) supplemented with 1% foetal bovine serum (Sigma-Aldrich, Madrid, Spain). The digested tissue was then gently triturated by suction using a glass pipette flamed on the tip to avoid cellular damage. Cell suspension was centrifuged for 2 min at 120xg. The supernatant was removed and the cells were resuspended in 5 mL Neurobasal medium and centrifuged again for 5 min to remove all the enzyme. Finally, the supernatant was replaced with fresh medium, the cells were resuspended and plated at a density of 120.000 cells/mL in poly-D-lysine (Sigma-Aldrich) 24-well plates (Nunc, Thermo Fisher Scientific, Madrid, Spain) in Neurobasal

medium supplemented with 1% foetal bovine serum and 2% B27 supplement (Gibco), to facilitate hippocampal neuron survival in vitro. Under these conditions the standard cell survival was 4 weeks and the experiments were performed on neurons of 8-15 days in culture.

In a few experiments on neurotoxicity, cortical neurons were prepared from rat embryo that were prepared essentially following the procedure used to prepare hippocampal neurons. Similar neurotoxicity experiments were performed in primary cultures of bovine adrenal chromaffin cells (BCCs) that were prepared as described by Moro et al. (1990) as well as in the tumoral cell line from human neuroblastoma SH-SY5Y that were prepared as previously described (Arias et al., 2005).

2.4.- Evaluation of cell viability

Cell viability was measured by quantitative colorimetric assay by using the MTT-based method (3-[4,5-dimethylthiazo1-2-y1]-2,5-diphenyltetrazolium bromide). MTT (Sigma-Aldrich) was added into the wells (0.5 mg/mL) and incubated at 37°C for 15 min. The tetrazolium ring of MTT can be cleaved by active dehydrogenases to produce a precipitated formazan that was solubilised with dimethyl sulfoxide (DMSO); cellular viability was quantified in a colorimetric reader at 560 nm (FLUOstar Optima, BMG, Germany). Data were expressed as percentage of MTT reduction, taking the maximum control tissue capability in each individual experiment as 100%.

2.5.- Neuronal viability experiments in rat hippocampal slices stressed with veratridine or glutamate

Experiments were performed at 37°C. Protocols are shown on top of the corresponding figures. Control and neurotoxicity groups were included in all experiments. Hippocampal slices were collected at the end of the experiment and incubated with MTT to determine cell viability. In experiments with veratridine, a positive control with tetrodotoxin (TTX, Tocris, Biogen Científica, Spain) was included.

2.6.- Cell viability experiments in rat hippocampal slices subjected to oxygen and glucose deprivation (OGD) plus reoxygenation

Following the period of stabilisation, slices were incubated for 15 min in an OGD buffer of the following composition (in mM): $CaCl_2$ 2, NaCl 120, KCl 2, $MgSO_4$ 1,19, KH_2PO_4 1,18; glucose was replaced by 11 mM 2-deoxy-glucose, equilibrated with a 95% N_2 and 5% CO_2 gas mixture. After this OGD period, slices were reoxygenated during 2 h in control buffer, bubbled with 95% O_2 and 5% CO_2 at 37°C, and finally cell viability was measured by MTT assay.

2.7.- Calcium measurements in populations of hippocampal neurons

Calcium measurements were performed with the selective calcium sensitive fluorescent dye Fluo-4 AM as previously described (Tenti et al., 2014). Briefly, Cells were plated into black 96-well plates at high density (45.000 cells/well). After removing the medium, cells were incubated with the Ca^{2+} fluorescent probe Fluo-4 (Gibco-Invitrogen) at 5 µM in Neurobasal Medium (Gibco-Invitrogen). After 45 min, cells were washed with Krebs-HEPES buffer of the following composition (in mM): NaCl 144, KCl 5.9, $MgCl_2$ 1.2, glucose 11, HEPES 10, pH 7.4). Compound was dissolved in the same buffer and incubated for 10 min. Fluorescence measurements were carried out on the fluorescence plate reader FLUOstar Optima (BMG Labtech GmbH; Ortemberg; Germany) using an excitation wavelength of 488 nm and recording the emission at 522 nm. Glutamate injection causes an increase in $[Ca^{2+}]_c$, and this leads to an increase in the emission fluorescence intensity of the probe.

2.8.- Measurement of ROS production

To measure the cellular production of reactive oxygen species (ROS), the molecular probe 2´,7´-dicholorofluorescein diacetate (H_2DCFDA) (Gibco-Invitrogen) was used. Hippocampal slices were loaded with 20 µM H_2DCFDA for 45 min at 37°C. H_2DCFDA diffuses through the cell membrane and is hydrolysed by intracellular esterases to the non-fluorescent form. This form reacts with intracellular ROS (including hydrogen peroxide, hydroxyl radicals and peroxynitrite) to form ROS

dichlorofluorescein, a green fluorescent dye. Fluorescence was measured in a fluorescence inverted NIKON eclipse T2000-U microscope (Nikon Europe B.V., Amsterdam, Netherlands). Wavelengths of excitation and emission for H_2DCFDA were 450 and 490 nm, respectively.

2.9.- Measurement of ATP in hippocampal slices

Intracellular ATP content was measured with a luminescence ATP Kinase-Glo® detection assay according to the manufacturer's instructions (Promega, Madrid, Spain). At the end of the experiment, hippocampal slices were disgregated by sonication (3-10 s, power 2) in 100 μl of potassium phosphate buffer (0.1 M, pH = 7.4), centrifuged and the supernatant was collected; 40 μl of the supernatant were placed in a white multiwell plate and 40 μl of the substrate was added into each well. Luminescence in each sample was measured with an Orion II microplate luminometer (Berthold, Germany). ATP content was normalized to the ATP content of control slices without any treatment.

2.10.- Intracellular GSH measurement

Hippocampal slices were treated as described for acute OGD/reox ischemia model as previously described (Egea et al., 2015). Briefly, to measure reduced glutathione (GSH) we selected monochlorobimane, a fluorescent dye that exhibits low fluorescent intensity when is unreacted; once it reacts with GSH it forms a highly fluorescent adduct (Fernandez-Checa and Kaplowitz, 1990) mediated by glutathione S-transferase (Kamencic et al., 2000). After the OGD/reox treatment, hippocampal slices were suspended in 50 μL potassium phosphate buffer and disgregated by sonication (3-10 s, power 2) in ice. The reaction started by the addition of monochlorobimane (100 μM) and glutathione S-transferase (0.5 U/mL) to a final volume of 100 μL. Fluorescence was measured in a FLUOstar optima microplate fluorescence reader (BMG technologies, Germany) at excitation and emission wavelengths of 410 and 485 nm respectively over 1 h at room temperature. Results were normalized to the basal conditions taken as 100 % GSH content.

2.11.- Western blot analysis

Slices of each experimental group were lysed in 100 μL ice-cold lysis buffer containing: 1% Nonidet P-40, 10% glycerol, 137 mM NaCl, 20 mM Tris-HCl, pH 7.5, 1 μg/mL leupeptin, 1 mM PMSF, 20 mM NaF, 1 mM sodium pyrophosphate and 1 mM Na_3VO_4. Proteins (30 μg) from these lysates were resolved by SDS-PAGE and transferred to Immobilon-P membranes (Millipore Millipore Corp.). Membranes were incubated with anti-HO-1 (1:1000), anti-GCLcat (1:1000) and anti-β-actin (1:50000) antibodies. Appropriate peroxidase-conjugated secondary antibodies (1:10000) were used to detect proteins by enhanced chemoluminescence. Protein bands were scanned and density was analysed using the Scion Image analysis software (Scion Corporation, NIH, Bethesda, MD, USA). Expression of HO-1 is presented as densitometric quantification using β-actin for normalisation.

2.12.- Recording of the spontaneous electrical activity of hippocampal neurons

Spontaneous postsynaptic currents (sPSCs), were recorded under voltage-clamp mode of the patch-clamp technique; the resting membrane potential (Vm) and the spontaneous action potentials (sAPs) were recorded under the current-clamp mode. The perforated-patch configuration of the patch-clamp technique was used in all cases.

Recordings were made with fire-polished electrodes (resistance 3-5 MΩ) mounted on the head stage of an EPC-9 patch-clamp amplifier (HEKA Elektronik, Lambrecht, Germany), allowing cancellation of capacitative transients and compensation for series resistance. Data were acquired at sampling frequencies ranging between 5 and 10 kHz and filtered at 1-2 kHz.

The perforated patch was obtained using pipettes containing 50-100 μg/mL amphotericin B (Sigma-Aldrich, Madrid, Spain) as permeabilising agent and a pipette-filling solution containing (in mM): NaCl, 10; K-glutamate, 120; Mg-ATP, 5; Na-GTP, 0.3; HEPES, 20; and EGTA, 14 (pH 7.2 with KOH). Amphotericin B was dissolved in DMSO and stored at -20°C in stock aliquots of 50 mg/mL. A fresh pipette solution was prepared every 2 h. To facilitate its sealing, the pipette was first dipped in a beaker

containing the internal solution and then back-filled with the same solution containing amphotericin B.

Recordings with leak currents >100 pA or series resistance >30 MΩ were discarded. Coverslips containing the cells were placed in an experimental chamber mounted on the stage of a Nikon T2000-U inverted microscope. The cell being recorded was locally, rapidly and continuously superfused with a Tyrode's solution containing (in mM): $CaCl_2$, 2; NaCl, 137; $MgCl_2$, 1; glucose, 10; KCl, 5; and HEPES-NaOH, 10 (pH 7.4). External solutions were rapidly exchanged using electronically driven miniature solenoid valves coupled to a multibarrel concentration-device, the common outlet of which was placed within 100 µm of the cell to be patched.

Data acquisition was performed using PULSE software (HEKA Elektronik). Data analysis was performed with the MiniAnalysis software (Synaptosoft, Leonia, NJ, USA). All experiments were performed at room temperature (22-24 °C).

2.13.- Statistical analysis

Data are expressed as mean ± standard error of the mean (SEM). Comparisons between experimental and control groups were performed by one-way ANOVA followed by Newman-keuls post-hoc test, as required. The Student's t test was also used for paired data comparisons (namely, control versus a given treatment) within the same experiment. Differences were considered to be statistically significant when $p \leq 0.05$. All statistical procedures were carried out using GraphPad Prism 5.0.

2.14.- Solutions and compounds

Both IG20 and glutamate (Sigma-Aldrich) are soluble in water, and the stock solutions were at the concentration of 10 mM and 1 M, respectively. Veratridine (Sigma-Aldrich) was dissolved in DMSO (Sigma-Aldrich) and stored at 10 mM. All solutions were stored in aliquots at -20°C. The final concentration of DMSO used (always <0.1%) did not cause cell toxicity.

3.- RESULTS

Most of the experiments here described were done in acutely isolated rat hippocampal slices and in primary cultures of rat hippocampal neurons prepared from the brains of E18 rat embryos. The use of slices implied a higher level of physiological and pathophysiological approaches to the neurotoxicity and neuroprotection studies. On the other hand, the patch-clamp studies requiring the recording of sPSCs at the single-cell level were done in cultures of rat embryo hippocampal neurons. Nevertheless, primary cultures of rat cortical neurons and bovine adrenal chromaffin cells, as well as some cultures of the human neuroblastoma cell line SH-SY5Y were used in some experiments aimed at testing the potential neurotoxic effects of compound IG20 (Supporting information).

3.1.- Effects of IG20 on neurotoxicity elicited by veratridine, glutamate and acute ischemia model in hippocampal slices

Veratridine has been used as a neurotoxic stressor to elicit a state of vulnerability and cell death associated to Na^+ and Ca^{2+} overload in rat embryo cortical neurons (Pauwels et al., 1990), in bovine chromaffin cells (Maroto et al., 1994; Nicolau et al., 2009), and in rat hippocampal slices (Nicolau et al., 2010).Thus, we performed an initial set of experiments to inquire whether compound IG20 exerted neuroprotection against the neurotoxic effects of veratridine in acutely isolated hippocampal slices.

We first performed a dose-dependent toxicity curve in our hippocampal slices model to test whether IG20 itself exerted neurotoxic effects on various cell cultures and in hippocampal slices. IG20 only had a clear toxic effects in SH-SY5Y cells at 300 μM. In hippocampal slices, BBCs or hippocampal neuronal cultures IG20 at 0.2-100 μM did not exhibit neurotoxic effects (see Fig. SI1 in Supporting information).

After an initial 30 min resting period, the slices were incubated with increasing concentrations of veratridine for 1 h; then, cell viability with the mitochondrial probe MTT was estimated (Fig. SI2A). We choose 10 μM veratridine that approximately caused 40% cell death, to perform the following experiments with veratridine and IG20.

In these experiments we used the protocol shown on top of Fig. 2A. Slices were exposed to increasing IG20 concentrations during the initial 30 min resting period; then they were exposed to continued IG20 plus 10 µM veratridine during an additional 60 min period that was followed by the MTT assay. In 6 triplicate experiments, veratridine decreased cell viability to 63.4 ± 3 % of the basal value ($p < 0.001$); cell viability increased to 77.3 ± 4 % in the presence of veratridine plus 0.3 µM IG20 ($p < 0.01$); the compound did not increase further this parameter at 1 and 10 µM. As expected, the blocker of voltage-dependent Na^+ channels TTX at 1 µM, fully antagonised the veratridine elicited cell damage (Fig. 2A). Under these conditions IG20 afforded 40 ± 6 % ($p< 0.05$) protection at 0.3 µM and 48.6 ± 8% ($p < 0.01$) protection at 10 µM (Fig. 2A).

The concept of neurotoxicity implies an excess glutamate release and/or the deficient removal of synaptic glutamate, which results in overactivation of NMDA and AMPA receptors, the cell overload with Na^+ and Ca^{2+}, and cell death (Lau and Tymianski, 2010; Zundorf and Reiser, 2011). Hence, the neuroprotective effects of IG20 on veratridine elicited Na^+ and Ca^{2+} overload and cell damage, prompted the experiments with glutamate. After protocol optimization (Fig. SI3B), we selected the toxicity induced by 4 mM glutamate after 2 h exposure and 2 h recovery (30.5 ± 0.8 % decreased viability) to test the potential neuroprotective effect of our compound.

IG20 at increasing concentrations was present only during the 2 h recovery period (see protocol on top of Fig. 2B). We found an improved significant cell viability at the IG20 concentrations of 0.3 (47.6 ± 9 %, $p< 0.01$) and 3 µM (51.6±13%, $p< 0.01$), but not at the concentrations of 1 and 10 µM that although they exhibited some tendency for improvement, these values did not reach the level of statistical significance (Fig. 2B).

It was of interest to inquire the possibility that IG20 could afford protection on *in vitro* models of transient cerebral ischemia. This was studied in hippocampal slices subjected to a transient period of OGD followed by another period of reoxygenation. In so doing, the excess ROS production will cause neuronal damage (Egea et al., 2007b). The protocol on top of Fig. 2C indicates the experimental steps that were followed; the increasing concentrations of IG20 were present at all stages of this protocol. We found a protective effect of the compound against cell tissue damage at all concentrations tested

(1, 3 and 10 μM). Hence, OGD reduced cell viability to 62.2 ± 1.7 % ($p < 0.001$). Cell viability was significantly increased to 76.3 ± 4.8 % ($p < 0.01$) at 1 μM IG20 and to 82.3 ± 4.2 % at 3 μM ($p < 0.001$) were the compound showed the best neuroprotective effect against toxicity elicited by OGD/reox. This effect was slightly reduced at 10 μM were compound IG20 increased cell viability to 75.2 ± 4.3 % ($p < 0.01$).

3.2.- IG20 reduces ROS production induced by glutamate and OGD/reox and prevents tissue depletion of GSH and ATP

In order to evaluate the mechanism of action involved in the neuroprotective effects of IG20 we first tested the possibility that the compound mitigated Ca^{2+} overload in neurons challenged with glutamate, as Ca^{2+} is linked to the neurotoxic effects of glutamate (Lau and Tymianski, 2010; Zundorf and Reiser, 2011). However, IG20 was not able to reduce the cytosolic Ca^{2+} elevations ($[Ca^{2+}]_c$] induced by glutamate (100 μM) at any concentration tested (0.1 to 10 μM) (see supporting information, Fig. SI3).

The protection exerted by IG20 against the neurotoxic effects of glutamate in hippocampal slices could be associated to the mitigation of excess ROS production. To test this possibility, we performed experiments with the same protocol to that followed in the neurotoxicity-neuroprotection experiments namely, the incubation of hippocampal slices for 2 h with 4 mM glutamate and in the experimental group of slices, an additional 2 h incubation period with 3 μM IG20. ROS production was monitored at the end of the experiment with the fluorescent probe H_2DCFDA, an indicator of the tissue concentration of ROS.

Fig. 3A shows representative micro-images on the relative fluorescence intensity as an index of tissue ROS production in basal conditions, in the presence of glutamate with 2 additional 2 h recovery period, and in tissues incubated first with glutamate for 2 h and then with IG20 (at 3 μM) during the recovery period. Glutamate induced a 62 ± 8 % increased of ROS production (Fig. 3C). Compound IG20 effectively reduced ROS production almost to basal levels (13.6 ± 0.8 % increase, $p < 0.01$).

We were also interested in evaluating ROS production induced by OGD/reox in hippocampal slices. Oxygen deprivation induces mitochondrial depolarization leading

to increased ROS production; furthermore, the reoxygenation period exacerbates the production of free radicals augmenting the neuronal damage. Fig. 3B shows representative micro-images of ROS production induced by OGD/reox in hippocampal slices in basal conditions, slices subjected to OGD/reox and slices treated with IG20 (3 μM) following the protocol described in Fig. 2C. Quantification of ROS production resulted in an increased fluorescence intensity induced by OGD/reox to 77.9 %. Compound IG20 significantly reduced the excess ROS production by 71.4 %, compared with OGD/reox treated slices ($p < 0.01$).

The first defence system against free radicals production inside the cell is glutathione (GSH), which reacts with free radicals and pro-oxidant species to avoid oxidative stress damage. Hippocampal slices were subjected to OGD/reox as described in Fig. 2C in absence or presence of IG20 (3 μM). At the end of the reoxygenation period, hippocampal slices were disaggregated and GSH content was measured with the fluorescent dye monochlorobimane. As shown in Fig. 3E, OGD/reox significantly reduced the levels of GSH to 77.7 ± 5.2 % ($p < 0.001$) compared with basal conditions. Interestingly, slices treated with compound IG20 maintained GSH levels (93.6 ± 4.0 %) compared with basal levels being able to recover 71.3 % ($p < 0.01$) of GSH depletion induced by OGD/reox insult.

On the other hand, mitochondrial depolarization during OGD induces an acute drop in ATP levels (Chen et al., 2010) that has been related with cell death observed in ischemia. To determine the potential abrogation of ATP decreased levels by IG20, ATP levels were determined. As shown in Fig. 3E, compared with basal slices, OGD/reox induced a marked decrease of ATP levels to 34.3 ± 6.6 % ($p < 0.001$). Slice incubation with 3 μM IG20 successfully maintained ATP levels at 58.0 ± 8.6 % ($p < 0.05$), being able to recover 36 % of ATP drop after OGD/reox.

3.3.- IG20 induces Nrf2/ARE phase II response and reduces iNOS expression in hippocampal slices subjected to OGD/reox toxic insult

Whether the antioxidant activity of IG20 was associated to the induction of HO-1 was investigated in rat hippocampal neuronal cultures. Cells were incubated with increasing concentrations of IG20 during 24 h at 37°C and HO-1 protein density was

estimated with western blot at the end of this incubation period. A prototype western blot is shown in Fig. 4A. IG20 (3 μM) augmented by 7.4-fold HO-1 concentration ($p < 0.01$) and 2.4-folds GCLcat concentration (Fig. 4B, $p < 0.05$) two of the most important neuroprotective and anti-oxidant enzymes regulated by the Nrf2/ARE pathway.

We also analysed the expression of the pro-inflammatory enzyme inducible NO synthase (iNOS). OGD/reox induces glial activation and therefore, iNOS expression is highly increased. Fig. 4C shows the induction of iNOS expression upon OGD/reox exposure, that augmented 2-fold compared with basal conditions; compound IG20 successfully reduced iNOS expression almost to basal levels, namely to 1.13-fold over basal ($p < 0.05$) indicating the anti-inflammatory potential of IG20.

3.4.- The neuroprotective effects of IG20 partially depend on the PI3K/Akt, ERK1/2 and Junk pathways

As described above, the mechanism of action by which compound IG20 exerts its neuroprotective effect against OGD/reox partially depends on the phase II antioxidant response. However, the expression of phase II antioxidant enzymes is time dependent and probably, there are other mechanisms of action that complement the neuroprotective profile of compound IG20. To further elucidate the participation of other neuroprotective pathways in the mechanism of action of IG20 we performed the OGD/reox protocol as described in Fig. 5A in presence of IG20 or IG20 combined with the Jak2/STAT3 inhibitor AG490, the MEK/ERK1/2 inhibitor PD98059 and the PI3K/Akt antagonist LY294002, at 10 μM each. Previously, we demonstrated that these inhibitors had no effect on cell death induced by OGD/reox (Buendia et al., 2015a; Buendia et al., 2015b). As shown in Fig. 5A, slices incubated with IG20 showed an increased cellular viability compared with those subjected only to OGD/reox insult (52.6 ± 2.1 % cell viability increase, $p < 0.001$). So, it seems that the mechanism of action of IG20 partially depends also on the Jak2/STAT3 pathway, on the ERK1/2 pathway and on the PI3K/Akt pathway as all three inhibitors tested partially reverted the neuroprotective effect of IG20 by 49.6 % (AG490, $p < 0.01$), 24.4 % (PD98059, $p < 0.05$) and 48.1 % (LY294002, $p < 0.05$), respectively.

To further demonstrate the involvement of these pathways in the neuroprotective effect of compound IG20 we used rat primary neuronal cultures. Neurons were incubated with the compound at 3 μM. Neurons were collected after 15 min, 30 min and 60 min incubation with IG20 and protein phosphorylation was evaluated by western blot. As shown in Fig. 5B and 5C, compound IG20 significantly increased the phosphorylation of ERK1/2 and Akt at the incubation time of 60 min (pERK1/2) and at 30 min incubation (Akt).

3.5.- Effects of IG20 on the spontaneous postsynaptic currents and action potentials in cultured hippocampal neurons

In a recent study we found that IG20 exerted a modulatory effect on Na^+ currents (I_{Na}) in bovine chromaffin cells (Crespo-Castrillo et al., 2015). Thus, it was possible that IG20 could also exhibit some actions on the sPSCs and on sAPs in hippocampal neuron cultures.

Under the voltage-clamp configuration of the patch-clamp technique, the example neuron of Fig. 6A fired sPSCs that are due to stimulation by glutamate and GABA of glutamatergic and gabaergic receptors (Arnaiz-Cot et al., 2008). This firing pattern lasts for several minutes and thus, the effects of 1 and 10 μM concentrations of IG20 on such sPSCs could be longitudinally tested within the same neuron. Note that 1 μM caused a mild but visible reduction in sPSCs frequency; at 10 μM, however, a drastic reduction in frequency and sPSCs amplitude was produced, an effect that was quickly reversed upon IG20 washout. Averaged data on normalised frequency amplitude, and integrated area of sPSCs are graphed in Fig. 6B, C and D. At 1 μM, IG20 reduced the frequency by 37 ± 4 % ($p < 0.05$), the amplitude by 17 ± 1.8 %, and the area by 35.2 ± 3.5 % ($p < 0.01$). At 10 μM, the reductions of the 3 parameters were 43.3 ± 5 % ($p < 0.01$) for the frequency, 43.8 ± 4 % ($p < 0.001$) for amplitude, and 61 ± 6 % ($p < 0.001$) for the area.

We also tested the effect of IG20 on the frequency of sAPs recorded in hippocampal neurons under the current-clamp configuration of the patch-clamp technique. Fig. 7A shows an example record of sAPs before or during the cell exposure to 1 and 10 μM IG20; note the mild reduction of AP frequency at 1 μM and the more drastic reduction of frequency and amplitude of the APs in the presence of 10 μM IG20,

a drastic effect that fully reversed upon its washout. Averaged data from 5 different neurons indicated that at 1 μM AP frequency was reduced by 41 ± 4 % ($p < 0.01$) and at 1 μM IG20 such reduction augmented to 65 ± 6 % ($p < 0.001$) (Fig. 7B).

4.-DISCUSSION

Central in this study was the finding that the novel synthetic sulfoglycolipid IG20 afforded neuroprotection in rat hippocampal slices whose neurons were made vulnerable with three different stressors namely, veratridine, glutamate, and OGD/reox (Fig. 2). We also found that by itself, IG20 did not cause cell damage in a wide range of concentrations and in 5 different cell models namely, rat cortical and hippocampal neurons, bovine chromaffin cells, rat hippocampal slices, and the cell line human neuroblastoma SH-SY5Y; only at the high concentrations of 30 μM in cortical neurons and 300 μM in SH-SY5Y cells, did IG20 cause notable damage (Fig. SI1, Supporting info). Of interest was the fact that IG20 augmented cell viability at 3-30 μM in SH-SY5Y cells and at 100 μM in bovine chromaffin cells (Fig. SI1, in Supporting information). These effects are in line with its neuritogenic effects that could be an indication of the capacity of IG20 to enhance synaptic plasticity (Garcia-Alvarez et al., 2015).

From a strict pharmacological point of view, it can be argued that the capacity of IG20 to preserve a better cell viability when hippocampal slices were incubated with the three stressors lacked a clear concentration-dependence. For instance, in the case of veratridine that elicited quite consistent neuronal damage, IG20 exhibited similar protection at the three concentrations used (0.3, 1 and 10 μM) (Fig. 2A). More unreliable where the results with glutamate where IG20 afforded significant protection at 0.3 and 3 μM but, surprisingly, at 1 and 10 μM there was no protection (Fig. 2A). Lastly, the protection afforded by IG20 against OGD neurotoxicity was observed at 1, 3 and 10 μM; however, in this case the neuroprotective profile of IG20 described a U-shaped concentration-dependence, a finding suggesting different activities at higher concentrations.

In previous studies we have found that the concentration-dependence of the neuroprotective effects of various compounds varies according to the cell/tissue model

and the biological targets for those agents. Thus, concentration-dependence was present when the targets were ion channels or transporters. This was the case for the nicotinic receptor agonist epibatidine in bovine chromaffin cells stressed with rotenone/oligomycin (Egea et al., 2007a), with the NMDA receptor blocker minocycline in rat hippocampal neurons stressed with glutamate (Gonzalez et al., 2007), or with CGP37157, a blocker of the mitochondrial Na^+/Ca^{2+} exchanger that also target various ion channels, in bovine chromaffin cells stressed with veratridine but not with rotenone/oligomycin (Nicolau et al., 2009) or in rat hippocampal slices stressed with veratridine (Nicolau et al., 2010). However, when the neuroprotective target is a given signalling pathway, the concentration-dependence of the compounds is poor or non-existent. This was the case for the neuroprotective effects of the PPARγ receptor agonist NP00111 and rosiglitazone, in rat hippocampal slices stressed with OGD (Rosa et al., 2008), the melatonin-sulforaphane hybrid ITH12674 in rat cortical neurons stressed with rotenone/oligomycin or with terbutyl hydroperoxide (Egea et al., 2015), or the multitarget ligand ITH33/IQM-21 in rat hippocampal slices stressed with OGD (Lorrio et al., 2013). Sulfoglycolipid IG20 seems to belong to this last group of compounds that exert neuroprotection through a mechanism that involves a given cellular signalling pathway. In line with this proposal are the various families of glycolipids and sulfoglycolipids synthesised at our laboratory that by acting on intracellular signalling pathways exhibit antimitotic activity in melanoma and glioma cells (Doncel-Perez et al., 2013; Garcia-Alvarez et al., 2007). In this line is IG20 that belongs to a new family of sulfoglycolipids that emerged in the context of the synthesis of new antineoplasic agents with potential therapeutic application in glioma and melanoma, and that promoted neuritic growth and myelination (Garcia-Alvarez et al., 2015). The question now arises on how these plastic effects of IG20 are linked to its neuroprotective effects in hippocampal slices here reported.

IG20 did not affect the $[Ca^{2+}]_c$ elevations triggered by glutamate in cortical neurons (Fig. SI3, Supporting information) and thus a direct action on NMDA/AMPA receptors can be discarded. An antioxidant effect of IG20 could explain its neuroprotective effects on the basis of two observations namely, its ability to mitigate the enhanced ROS production in hippocampal slices stressed with glutamate (Fig. 3C and B) or OGD/reox (Fig. 3D) and its capacity to induce the expression of HO-1 (Fig. 4A) and GCLcat (Fig. 4B). Mitigation of ROS production by some agents have been

taken as the basic changes that activate neuroprotective pathways in, for instance, chromaffin cells (Egea et al., 2007a) or in cortical neurons stressed with rotenone/oligomycin (Egea et al., 2015). Furthermore, blockade of ROS production by compound IG20 might induce a stabilization of GSH levels (Fig. 3E) avoiding its consumption by radical species. Thus, the reduction of radical species and the augmentation of GSH levels can improve mitochondrial function facilitating the stabilisation of the membrane potential, favouring the maintenance of ATP levels (Fig. 3F) and cellular metabolism.

As mentioned before, compound IG20 is able to increase the expression of HO-1 and GCLcat in rat primary neuronal cultures after 24 incubation. The ability to induce the Nrf2/ARE pathway of compound IG20 might be also related with the activation of phase II antioxidant response that induces the expression of antioxidant and anti-inflammatory enzymes on the other hand, the previously described activity of IG20 over glial cells (García-Alvarez *et al.*, 2015) might be responsible for the reduction of iNOS expression upon OGD/reox treatment (Fig. 4D).

The Nrf2/ARE pathway might be activated by different mechanisms such as electrophilic modification of Keap1 cysteine residues, by the phosphorylation of different kinases related with neuroprotective pathways or by receptor activation (Buendia et al., 2015b; Chen et al., 2010). IG20 increased ERK1/2 and Akt phosphorylation (Fig. 5B and C). Akt is known to phosphorylate GSK3β at Ser-9 (Cuchillo-Ibanez et al., 2013; Stambolic and Woodgett, 1994) to inactivate it, promoting Nrf2 stabilization and activation of the phase II response (Salazar et al., 2006). Thus, the connection between Akt phosphorylation, Nrf2 induction and the reduction of iNOS expression is the most plausible neuroprotective pathway that explains the neuroprotective effects of IG20.

An interesting finding was the reduction by IG20 of the sPSCs frequency and amplitude (Fig. 6) and the reduction of sAPs frequency (Fig. 7), meaning that neuronal excitability is decreased in the presence of the compound. In a previous study performed in primary cultures of hippocampal neurons, we found that the neuroprotective effects of minocycline could be associated to the mitigation of neuronal excitability, to partial blockade of inward Na^+ and Ca^{2+} currents, and to decrease Ca^{2+} overloading (Gonzalez et al., 2007). Thus, the IG20 neuroprotective effects could in part be explained through

mitigation of neuronal excitability, as the case is for minocycline. However, unlike minocycline, IG20 did not affect the glutamate elicited $[Ca^{2+}]_c$ elevations (Fig. SI3, Supporting information). In bovine chromaffin cells we found that IG20 augmented I_{Na} and the large conductance Ca^{2+} dependent outward K^+ currents (BK channels) and the exocytotic release of catecholamine without I_{Ca} alteration (Crespo-Castrillo et al., 2015). Nevertheless, this pharmacological profile in bovine chromaffin cells may not explain the neuroprotective effects of IG20 here described.

Sulfoglycolipid IG20 contains a polar sugar moiety carrying a negatively charged OSO_3^{-1} group. This could explain our previous finding that the fluorescent derivative IG20-NBD remains confined to the plasmalemma of chromaffin cells and does not enter into the cell cytosol (Crespo-Castrillo et al., 2015). This suggests that the neuroprotection exerted by IG20 may be linked to a membrane-delimited effect. Ig20 has a molecular structure that reminds the endogenous sulfatide (Fig. 1). Glycolipids are predominantly located in the outer plasmalemma layer. Their sulfation introduces negative charges that are determinants for interactions with proteic receptors and ion channels that might explain the induction of phosphorylation of ERK1/2 and Akt. Thus, the neuroprotective effects of IG20 could find an explanation in the context of caveola, that are lipid raft domains (Simons and Ikonen, 1997). Raft-enriched lipids such as cholesterol and sphingolipids can interact with membrane proteins to regulate the activities of ion channels (Dart, 2010). Also, ceramide and sphingosine regulate membrane fusion (exocytosis) and fission endocytosis processes (Darios et al., 2009; Rosa et al., 2010). Glycolipids are known to be located at the outer plasmalemma layer and their sulfation introduces negative charges that are determinants for their interactions with proteic receptors and ion channels. They contribute to the regulation of cell differentiation, development, cell adhesion, or immune responses (Honke, 2013). Additionally, the sulfoglycolipid sulfatide plays a critical role in the regulation of oligodendrocytes differentiation and the maintenance of myelin and axonal structure (Marcus et al., 2006). Furthermore, altered sphingolipid metabolism has been found in some sphingolipidoses, atherosclerosis, diabetes, and cancer (Delgado et al., 2007), as well as in early Alzheimer's disease (Han et al., 2002). Hence, our synthetic compound IG20 rises the possibility of regulating some of those physiological and pathological processes by using exogenous sulfoglycolipids that promote neuritic growth and myelination, inhibit astroglia and microglia proliferation (Garcia-Alvarez et al., 2015),

and favour the exocytotic release of neurotransmitters (Crespo-Castrillo et al., 2015). To this interesting pharmacological profile, we can now add the IG20 neuroprotective effects.

In conclusion, the novel synthetic sulfoglycolipid IG20 exhibits neuroprotective properties in rat hippocampal slices challenged with various stressors. Such effect is likely due to its ability to activate the phase II antioxidant response.

5.-ACKNOWLEDGMENTS

This study was supported by a grant from Ministerio de Economía y Competitividad, Spain (MINECO SAF2013-44108-P to AGG and LG; MAT2015-65184-C2-2-R to AFM, CABICYC UAM-Bioibérica and European Commission-ERC, People (Marie Curie Actions) FP7 under REA grant agreement n° PCIG11-GA-2012-322156; Spanish Ministry of Health (Instituto de Salud Carlos III) (grant PI14/00372) and Miguel Servet (CP11/00165); Bayer A.G., "From Targets to Novel Drugs" program (grant 2015-03-1282) and Fundación FIPSE (grant 12-00001344-15) to RL. RL thanks IS Carlos III for research contract under Miguel Servet Program. P.M. thanks MECD for FPU fellowship (AP2010-1219). We thank the continued support of Fundación Teófilo Hernando. The authors have no conflict of interest to declare.

FIGURE LEGENDS

Figure 1. Molecular structures of endogenous sulfatide and compound IG20 (oleoyl 2-N-acetyl-2-amino-2-deoxy-6-O-(oxosulfonyl)-alpha-D-glucopyranoside).

Figure 2: Neuroprotection elicited by IG20 against neurotoxicity elicited by veratridine (VTD), glutamate (Glu) and oxygen plus glucose deprivation followed by reoxygenation (OGD/reox) in rat hippocampal slices. (A) Experimental protocol consists of 30-min preincubation period with IG20 at different concentrations, and one hour co-incubation with IG20 and VTD.. (B) Neuroprotection elicited by different concentrations of IG20, expressed in the ordinate as cell viability. Experimental protocol consists in 2 h incubation with glutamate (4 mM) followed by 2 h incubation with different concentrations of IG20 in the absence of glutamate. (C) Neuroprotection elicited by IG20 against toxicity induced by OGD/reox. The experimental protocol consists in 30-min preincubation period with IG20 at different concentrations, 15-min under OGD in the presence of IG20 and 2 h of reoxygenation with IG20 at the same concentrations. MTT reduction measurement, as an indicator of cell viability, is expressed in the ordinates as percentage of control. Data are means ± SEM of 6 triplicate experiments. ###$p<0.001$ with respect to basal, *$p<0.05$ and **$p<0.01$, ***$p<0.01$ with respect to the elicited neuronal damage by each toxic insult.

Figure 3: IG20 drastically reduces the production of reactive oxygen species (ROS) in hippocampal slices subjected to glutamate or OGD/reox-induced cellular damage and prevents depletion of GSH and ATP induced by OGD/reox. (A and B) Representative microphotographs (100X) under each experimental condition in the CA1 hippocampal region. (C) Quantification of the ROS production in CA1 after 2 h incubation with glutamate (4 mM) followed by 2 h IG20 incubation at the concentration of 3 μM. (D) Mean ROS production in CA1 after 15 min OGD followed by 2 h reox with IG20 incubation at the concentration of 3 μM. Data were normalised by nuclei staining with Hoechst dye. (E) GSH levels and (F) ATP levels measured after OGD/reox in presence or absence of 3 μM IG20. Values correspond to

means ± SEM of 3 or 4 triplicate experiments performed in hippocampal slices from different animals. ##p<0.01 ###p<0.001 with respect to basal; *p<0.05, **p<0.01, ***p<0.001 with respect to the corresponding toxic alone.

Figure 4: IG20 induces Nrf2/ARE pathway activation in primary neuronal cultures and hippocampal slices and reduces iNOS expression after OGD/reox toxic insult. (A) HO-1 induction induced by compound IG20 in hippocampal neuronal cultures. Neurons were treated with IG20 (3 μM) during 24 h. Thereafter, cells were collected and HO-1 expression was evaluated by western blot analysis. (B) GCLcat induction elicited by exposure of neuronal cultures to 3 μM IG20. (C) iNOS expression induced by OGD/reox and reduction induced by compound IG20. At the end of the experiment slices were collected and protein expression was analysed by western blot. Values correspond to means ± SEM of 5 triplicate experiments performed in three different cultures (panels A and B) and 4 experiments in slices subjected to OGD/reox (panel C). #p<0.05, ##p<0.01 with respect to basal conditions; *p<0.05 with respect to OGD/reox alone.

Figure 5: Jak2/Stat3, PI3K/Akt and ERK1/2 survival pathways are involved in the neuroprotective effects of IG20 against OGD/reox neurotoxicity. (A) The neuroprotective effect of IG20 was partially reverted by 10 μM of the inhibitors of the signalling pathways Jak2/STAT3 (AG490, AG), ERK1/2 (PD98059, PD), and PI3K/Akt (LY294002; LY). The experimental protocol is depicted in the top part of the panel. Data are expressed as mean ± SEM of 7 different experiments. *###p<0.001* with respect to basal; **p<0.05, **p<0.01, ***p<0.001* with respect to OGD/reox alone. (B) ERK1/2 phosphorylation induced by IG20 (3 μM) in primary rat neuronal cultures after 15, 30 and 60 min incubation measured by western blot. (C) Akt phosphorylation induced by IG20 (3 μM) in primary rat neuronal cultures after 15, 30 and 60 min incubation measured by western blot. Data are expressed as means ± SEM of 6 different experiments in triplicate; *p<0.05, **p<0.01, *** p<0.001 with respect to basal.

Figure 6: Effects of compounds IG20 on spontaneous postsynaptic currents (sPSCs) in voltage-clamped hippocampal neurons. (A) Representative traces of an original record in the voltage-clamp configuration of the patch-clamp technique, with the holding potential fixed at -80 mV. Plot of normalised frequency (B), amplitude (C), and area (D) of sPSCs, calculated at 10-s periods with respect to control. Experimental conditions are indicated by the horizontal bars at the bottoms of panels B, C, and D. Data are means±SEM of the number of cells and cultures shown in parentheses. *$p<0.05$, **$p<0.01$, and ***$p<0.001$ with respect to control.

Figure 7: Sulfoglycolipid IG20 reduces the frequency of spontaneous action potentials (sAPs) in current-clamped hippocampal neurons. (A) Records from an example neuron, and the effects of IG20 applied at the indicated concentrations and time periods indicated by the bottom horizontal bars. (B) Normalised frequency of sAPs under control conditions, and in the presence of 1 or 10 μM IG20. Data are means ± SEM of the number of cells shown in parentheses. **$p<0.01$, and ***$p<0.001$ with respect to control.

REFERENCES

Arias, E., Gallego-Sandin, S., Villarroya, M., Garcia, A. G., Lopez, M. G., 2005. Unequal neuroprotection afforded by the acetylcholinesterase inhibitors galantamine, donepezil, and rivastigmine in SH-SY5Y neuroblastoma cells: role of nicotinic receptors. J Pharmacol Exp Ther 315, 1346-1353.

Arnaiz-Cot, J. J., Gonzalez, J. C., Sobrado, M., Baldelli, P., Carbone, E., Gandia, L., Garcia, A. G., Hernandez-Guijo, J. M., 2008. Allosteric modulation of alpha 7 nicotinic receptors selectively depolarizes hippocampal interneurons, enhancing spontaneous GABAergic transmission. Eur J Neurosci 27, 1097-1110.

Buendia, I., Egea, J., Parada, E., Navarro, E., Leon, R., Rodriguez-Franco, M. I., Lopez, M. G., 2015a. The melatonin-N,N-dibenzyl(N-methyl)amine hybrid ITH91/IQM157 affords neuroprotection in an in vitro Alzheimer's model via hemo-oxygenase-1 induction. ACS Chem Neurosci 6, 288-296.

Buendia, I., Gomez-Rangel, V., Gonzalez-Lafuente, L., Parada, E., Leon, R., Gameiro, I., Michalska, P., Laudon, M., Egea, J., Lopez, M. G., 2015b. Neuroprotective mechanism of the novel melatonin derivative Neu-P11 in brain ischemia related models. Neuropharmacology 99, 187-195.

Chen, X., Kintner, D. B., Baba, A., Matsuda, T., Shull, G. E., Sun, D., 2010. Protein aggregation in neurons following OGD: a role for Na+ and Ca2+ ionic dysregulation. J Neurochem 112, 173-182.

Cheng, H., Wang, M., Li, J. L., Cairns, N. J., Han, X., 2013. Specific changes of sulfatide levels in individuals with pre-clinical Alzheimer's disease: an early event in disease pathogenesis. J Neurochem 127, 733-738.

Coetzee, T., Fujita, N., Dupree, J., Shi, R., Blight, A., Suzuki, K., Popko, B., 1996. Myelination in the absence of galactocerebroside and sulfatide: normal structure with abnormal function and regional instability. Cell 86, 209-219.

Crespo-Castrillo, A., Punzon, E., de Pascual, R., Maroto, M., Padin, J. F., Garcia-Alvarez, I., Nanclares, C., Ruiz-Pascual, L., Gandia, L., Fernandez-Mayoralas, A., Garcia, A. G., 2015. Novel synthetic sulfoglycolipid IG20 facilitates exocytosis in chromaffin cells through the regulation of sodium channels. J Neurochem 135, 880-896.

Cuchillo-Ibanez, I., Balmaceda, V., Botella-Lopez, A., Rabano, A., Avila, J., Saez-Valero, J., 2013. Beta-amyloid impairs reelin signaling. PLoS One 8, e72297.

Darios, F., Wasser, C., Shakirzyanova, A., Giniatullin, A., Goodman, K., Munoz-Bravo, J. L., Raingo, J., Jorgacevski, J., Kreft, M., Zorec, R., Rosa, J. M., Gandia, L., Gutierrez, L. M., Binz, T., Giniatullin, R., Kavalali, E. T., Davletov, B., 2009. Sphingosine facilitates SNARE complex assembly and activates synaptic vesicle exocytosis. Neuron 62, 683-694.

Dart, C., 2010. Lipid microdomains and the regulation of ion channel function. J Physiol 588, 3169-3178.

Delgado, A., Casas, J., Llebaria, A., Abad, J. L., Fabrias, G., 2007. Chemical tools to investigate sphingolipid metabolism and functions. ChemMedChem 2, 580-606.

Doncel-Perez, E., Garcia-Alvarez, I., Fernandez-Mayoralas, A., Nieto-Sampedro, M., 2013. Synthetic glycolipids for glioma growth inhibition developed from neurostatin and NF115 compound. Bioorg Med Chem Lett 23, 435-439.

Egea, J., Buendia, I., Parada, E., Navarro, E., Rada, P., Cuadrado, A., Lopez, M. G., Garcia, A. G., Leon, R., 2015. Melatonin-sulforaphane hybrid ITH12674 induces neuroprotection in oxidative stress conditions by a 'drug-prodrug' mechanism of action. Br J Pharmacol 172, 1807-1821.

Egea, J., Rosa, A. O., Cuadrado, A., Garcia, A. G., Lopez, M. G., 2007a. Nicotinic receptor activation by epibatidine induces heme oxygenase-1 and protects chromaffin cells against oxidative stress. J Neurochem 102, 1842-1852.

Egea, J., Rosa, A. O., Sobrado, M., Gandia, L., Lopez, M. G., Garcia, A. G., 2007b. Neuroprotection afforded by nicotine against oxygen and glucose deprivation in hippocampal slices is lost in alpha7 nicotinic receptor knockout mice. Neuroscience 145, 866-872.

Fernandez-Checa, J. C., Kaplowitz, N., 1990. The use of monochlorobimane to determine hepatic GSH levels and synthesis. Anal Biochem 190, 212-219.

Fernandez-Mayoralas, A., De La Figuera, N., Zurita, M., Vaquero, J., Abraham, G. A., San Roman, J., Nieto-Sampedro, M., 2003. Central neural tumor destruction by controlled release of a synthetic glycoside dispersed in a biodegradable polymeric matrix. J Med Chem 46, 1286-1288.

Garcia-Alvarez, I., Corrales, G., Doncel-Perez, E., Munoz, A., Nieto-Sampedro, M., Fernandez-Mayoralas, A., 2007. Design and synthesis of glycoside inhibitors of glioma and melanoma growth. J Med Chem 50, 364-373.

Garcia-Alvarez, I., Fernandez-Mayoralas, A., Moreno-Lillo, S., Sanchez-Sierra, M., Nieto-Sampedro, M., Doncel-Perez, E., 2015. Inhibition of glial proliferation, promotion of axonal growth and myelin production by synthetic glycolipid: A new approach for spinal cord injury treatment. Restor Neurol Neurosci 33, 895-910.

Gonzalez, J. C., Egea, J., Del Carmen Godino, M., Fernandez-Gomez, F. J., Sanchez-Prieto, J., Gandia, L., Garcia, A. G., Jordan, J., Hernandez-Guijo, J. M., 2007. Neuroprotectant minocycline depresses glutamatergic neurotransmission and Ca(2+) signalling in hippocampal neurons. Eur J Neurosci 26, 2481-2495.

Han, X., D, M. H., McKeel, D. W., Jr., Kelley, J., Morris, J. C., 2002. Substantial sulfatide deficiency and ceramide elevation in very early Alzheimer's disease: potential role in disease pathogenesis. J Neurochem 82, 809-818.

Honke, K., 2013. Biosynthesis and biological function of sulfoglycolipids. Proc Jpn Acad Ser B Phys Biol Sci 89, 129-138.

Kamencic, H., Lyon, A., Paterson, P. G., Juurlink, B. H., 2000. Monochlorobimane fluorometric method to measure tissue glutathione. Anal Biochem 286, 35-37.

Lau, A., Tymianski, M., 2010. Glutamate receptors, neurotoxicity and neurodegeneration. Pflugers Arch 460, 525-542.

Lorrio, S., Gomez-Rangel, V., Negredo, P., Egea, J., Leon, R., Romero, A., Dal-Cim, T., Villarroya, M., Rodriguez-Franco, M. I., Conde, S., Arce, M. P., Roda, J. M., Garcia, A. G., Lopez, M. G., 2013. Novel multitarget ligand ITH33/IQM9.21 provides neuroprotection in in vitro and in vivo models related to brain ischemia. Neuropharmacology 67, 403-411.

Marcus, J., Honigbaum, S., Shroff, S., Honke, K., Rosenbluth, J., Dupree, J. L., 2006. Sulfatide is essential for the maintenance of CNS myelin and axon structure. Glia 53, 372-381.

Maroto, R., De la Fuente, M. T., Artalejo, A. R., Abad, F., Lopez, M. G., Garcia-Sancho, J., Garcia, A. G., 1994. Effects of Ca2+ channel antagonists on chromaffin cell death and cytosolic Ca2+ oscillations induced by veratridine. Eur J Pharmacol 270, 331-339.

Moro, M. A., López, M. G., Gandía, L., Michelena, P., García, A. G., 1990. Separation and culture of living adrenaline- and noradrenaline-containing cells from bovine adrenal medullae. Anal Biochem 185, 243-248.

Nicolau, S. M., de Diego, A. M., Cortés, L., Egea, J., González, J. C., Mosquera, M., López, M. G., Hernández-Guijo, J. M., García, A. G., 2009. Mitochondrial Na^+/Ca^{2+}-exchanger blocker CGP37157 protects against chromaffin cell death elicited by veratridine. J Pharmacol Exp Ther 330, 844-854.

Nicolau, S. M., Egea, J., López, M. G., García, A. G., 2010. Mitochondrial Na^+/Ca^{2+} exchanger, a new target for neuroprotection in rat hippocampal slices. Biochem Biophys Res Commun 400, 140-144.

Nieto-Sampedro, M., 1988. Astrocyte mitogen inhibitor related to epidermal growth factor receptor. Science 240, 1784-1786.

Nieto-Sampedro, M., Broderick, J. T., 1989. A soluble brain molecule related to epidermal growth factor receptor is a mitogen inhibitor for astrocytes. J Neurosci Res 22, 28-35.

Pauwels, P. J., Van Assouw, H. P., Peeters, L., Leysen, J. E., 1990. Neurotoxic action of veratridine in rat brain neuronal cultures: mechanism of neuroprotection by Ca++ antagonists nonselective for slow Ca++ channels. J Pharmacol Exp Ther 255, 1117-1122.

Rosa, A. O., Egea, J., Martinez, A., Garcia, A. G., Lopez, M. G., 2008. Neuroprotective effect of the new thiadiazolidinone NP00111 against oxygen-glucose deprivation in rat hippocampal slices: implication of ERK1/2 and PPARgamma receptors. Exp Neurol 212, 93-99.

Rosa, J. M., Gandia, L., Garcia, A. G., 2010. Permissive role of sphingosine on calcium-dependent endocytosis in chromaffin cells. Pflugers Arch 460, 901-914.

Salazar, M., Rojo, A. I., Velasco, D., de Sagarra, R. M., Cuadrado, A., 2006. Glycogen synthase kinase-3beta inhibits the xenobiotic and antioxidant cell response by direct phosphorylation and nuclear exclusion of the transcription factor Nrf2. J Biol Chem 281, 14841-14851.

Simons, K., Ikonen, E., 1997. Functional rafts in cell membranes. Nature 387, 569-572.

Stambolic, V., Woodgett, J. R., 1994. Mitogen inactivation of glycogen synthase kinase-3 beta in intact cells via serine 9 phosphorylation. Biochem J 303 (Pt 3), 701-704.

Tenti, G., Parada, E., Leon, R., Egea, J., Martinez-Revelles, S., Briones, A. M., Sridharan, V., Lopez, M. G., Ramos, M. T., Menendez, J. C., 2014. New 5-unsubstituted dihydropyridines with improved CaV1.3 selectivity as potential neuroprotective agents against ischemic injury. J Med Chem 57, 4313-4323.

Valle-Argos, B., Gomez-Nicola, D., Nieto-Sampedro, M., 2010. Synthesis and characterization of neurostatin-related compounds with high inhibitory activity of glioma growth. Eur J Med Chem 45, 2034-2043.

Yiu, G., He, Z., 2006. Glial inhibition of CNS axon regeneration. Nat Rev Neurosci 7, 617-627.

Zhang, M., An, C., Gao, Y., Leak, R. K., Chen, J., Zhang, F., 2013. Emerging roles of Nrf2 and phase II antioxidant enzymes in neuroprotection. Prog Neurobiol 100, 30-47.

Zundorf, G., Reiser, G., 2011. Calcium dysregulation and homeostasis of neural calcium in the molecular mechanisms of neurodegenerative diseases provide multiple targets for neuroprotection. Antioxid Redox Signal 14, 1275-1288.

Figure 1

Click here to download high resolution image

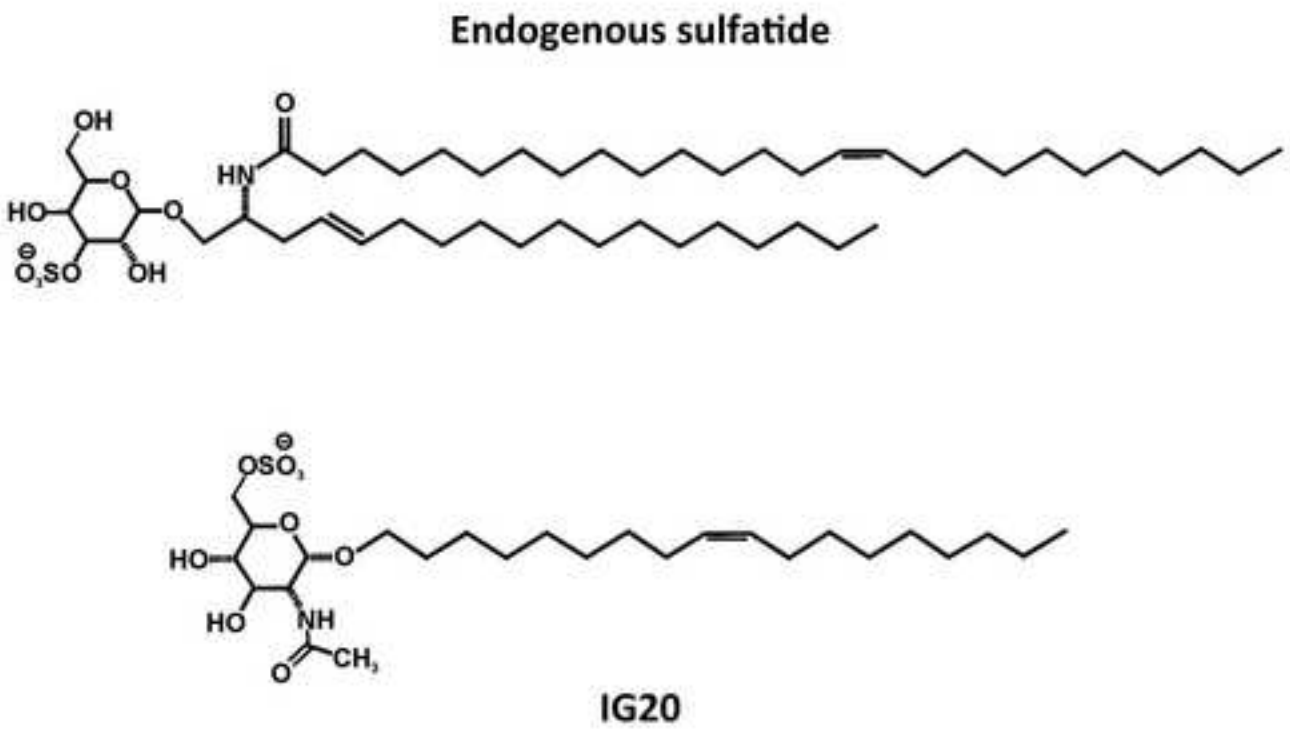

Figure 2

Click here to download high resolution image

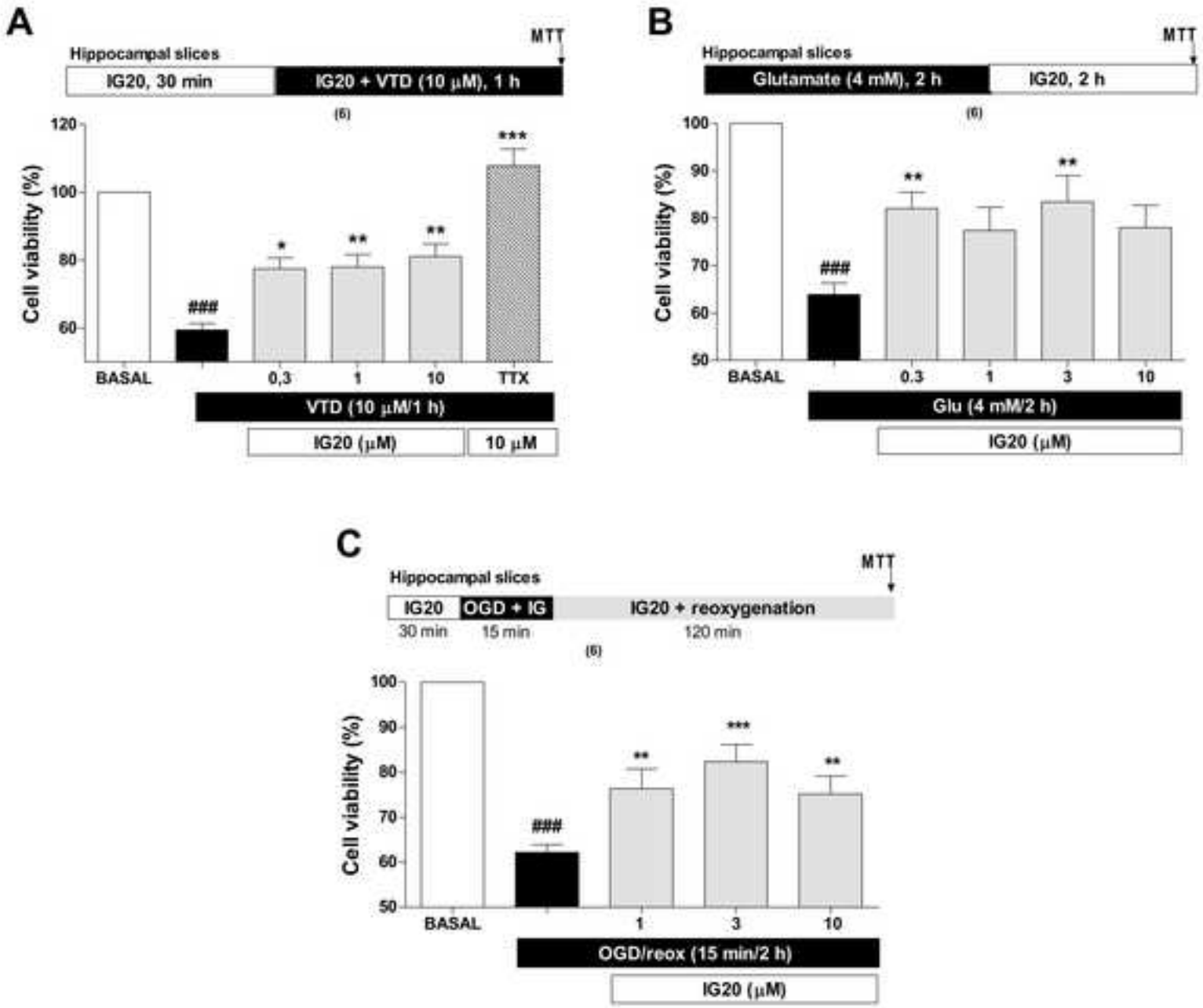

Figure3

Click here to download high resolution image

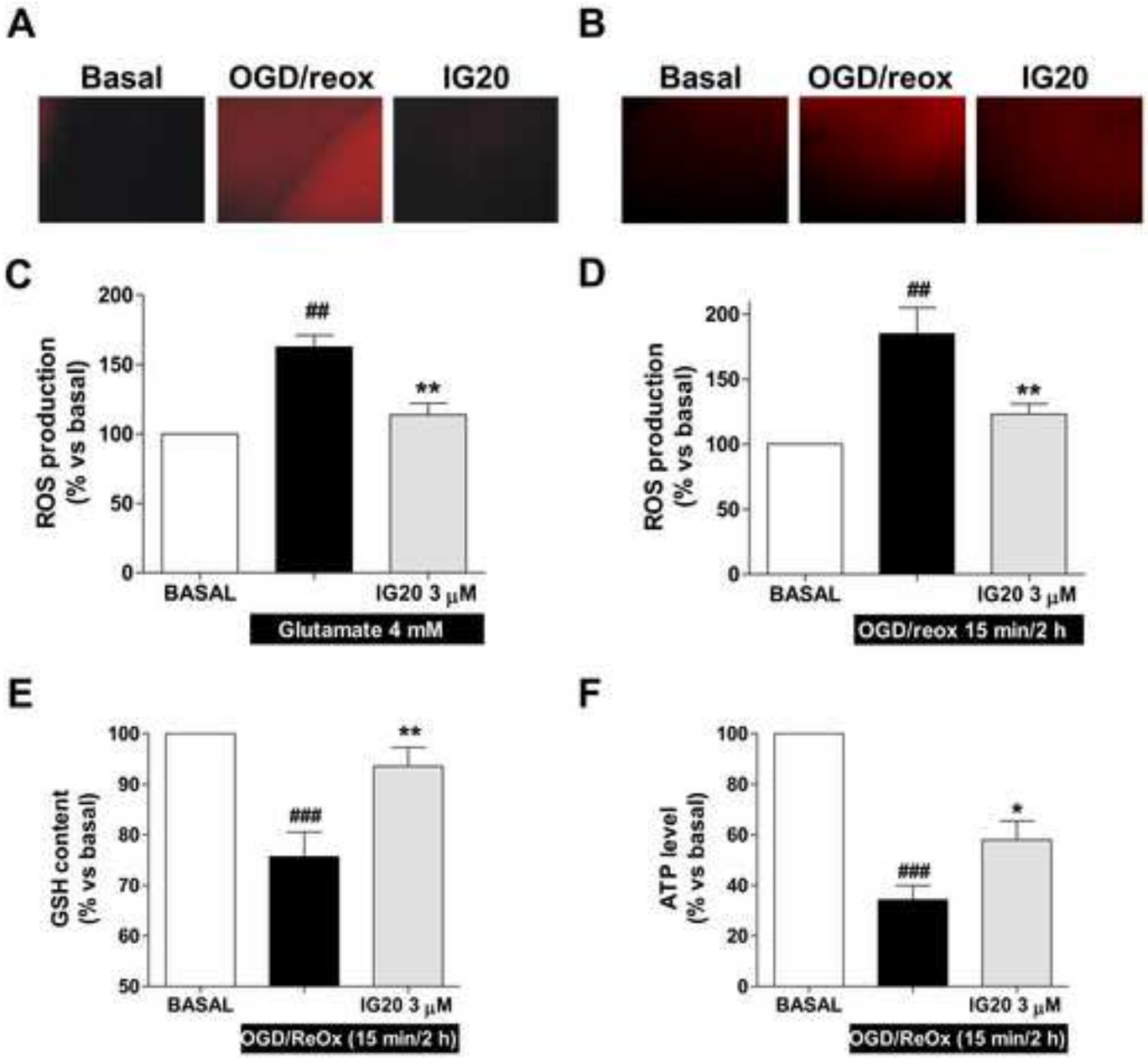

Figure 4

Click here to download high resolution image

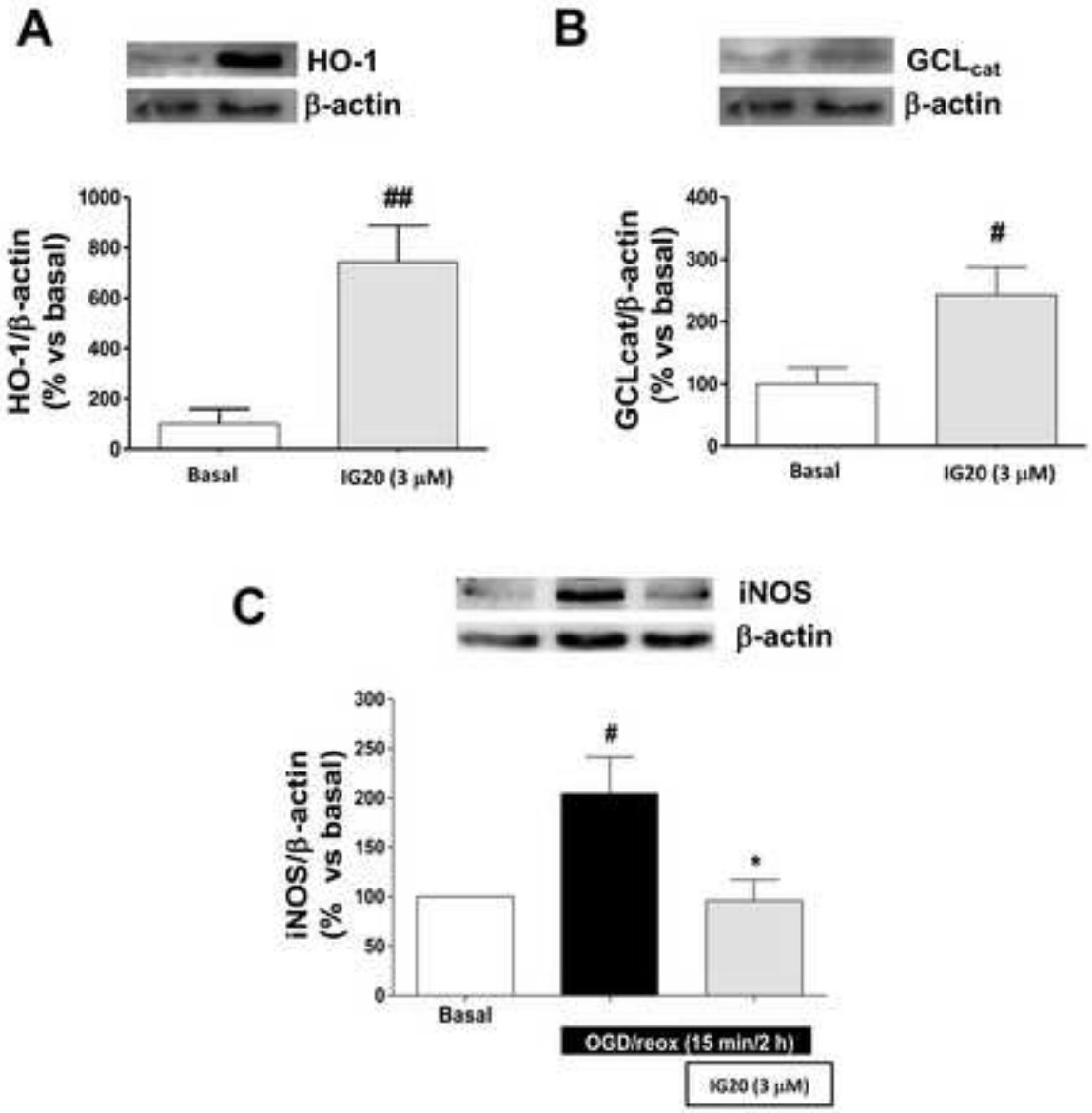

Figure 5

Click here to download high resolution image

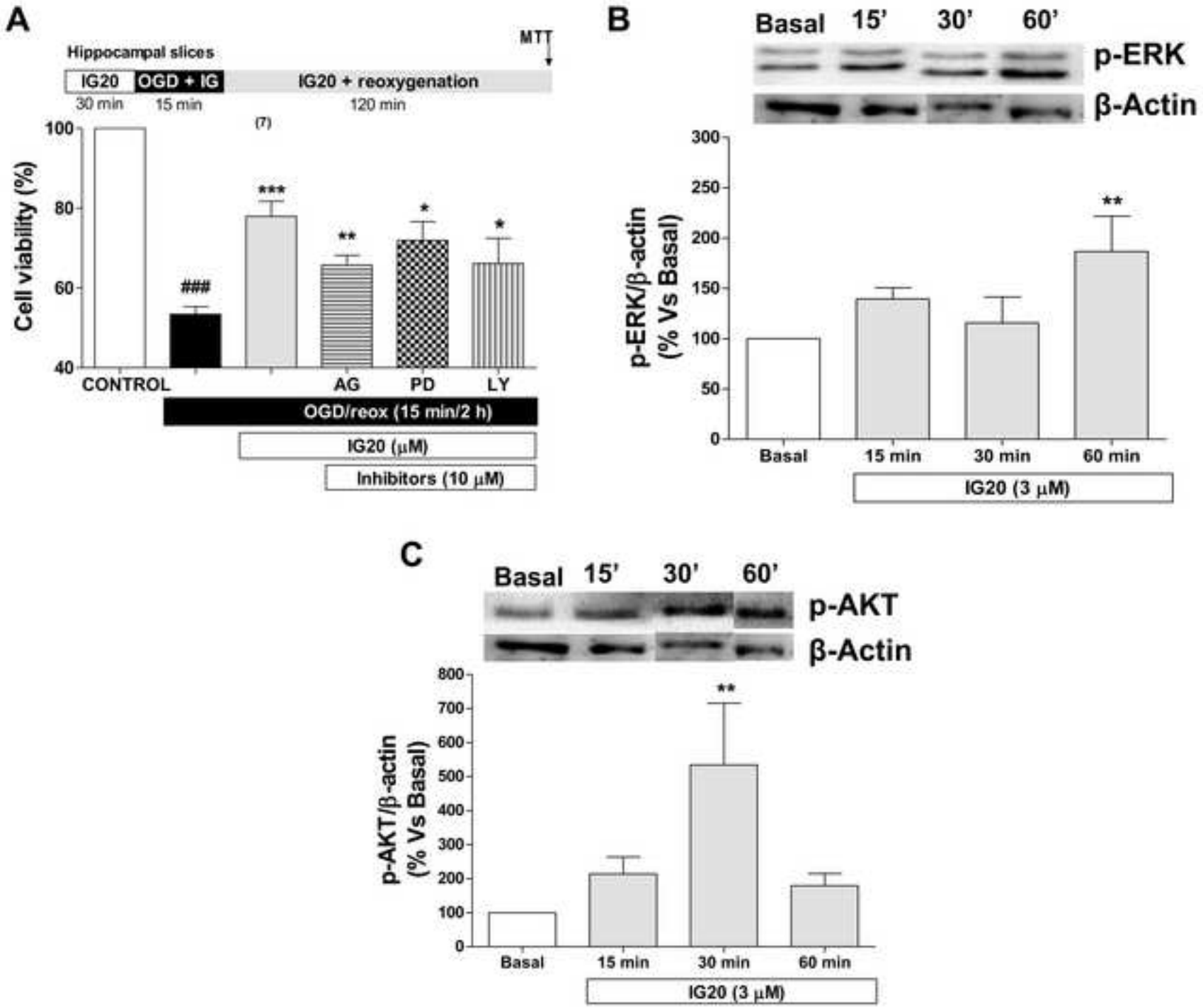

Figure 6

Click here to download high resolution image

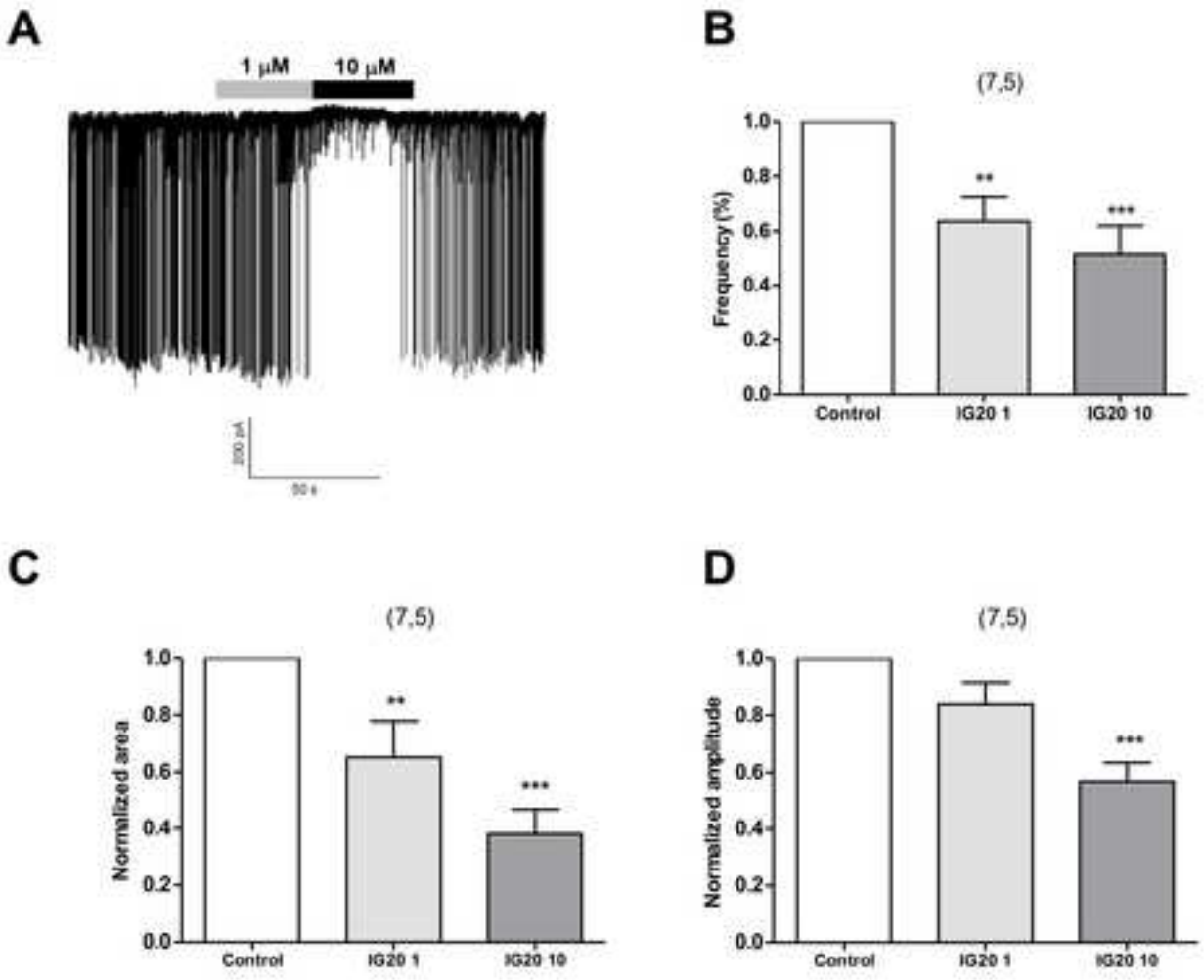

Figure 7

Click here to download high resolution image

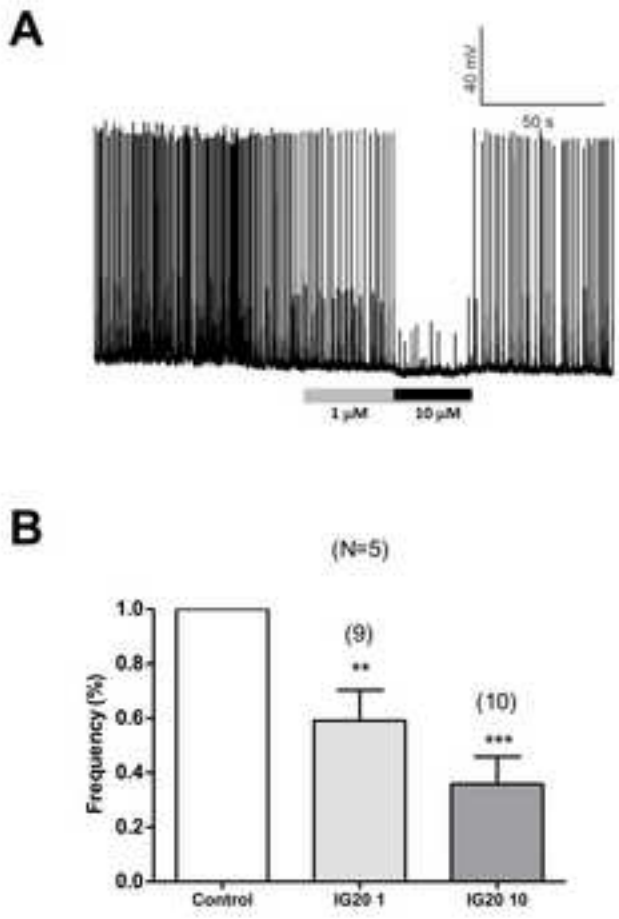

Figure SI1

Click here to download high resolution image

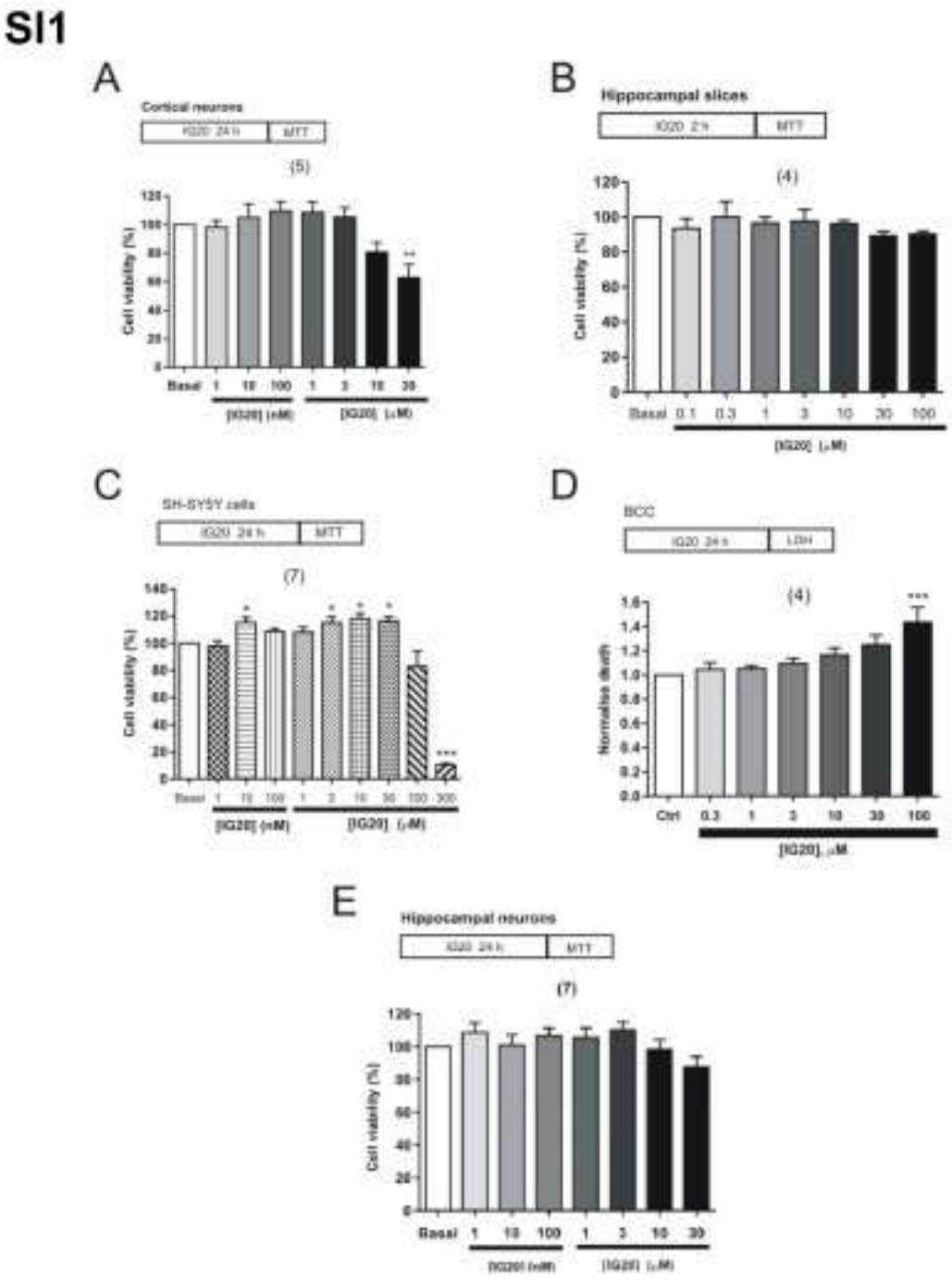

Figure SI2

Click here to download high resolution image

SI2

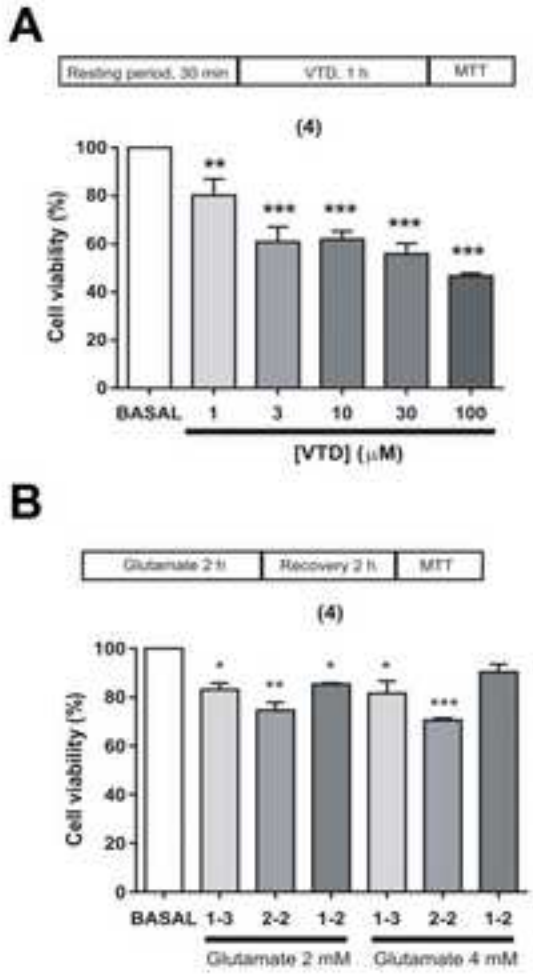

Figure SI3
Click here to download high resolution image

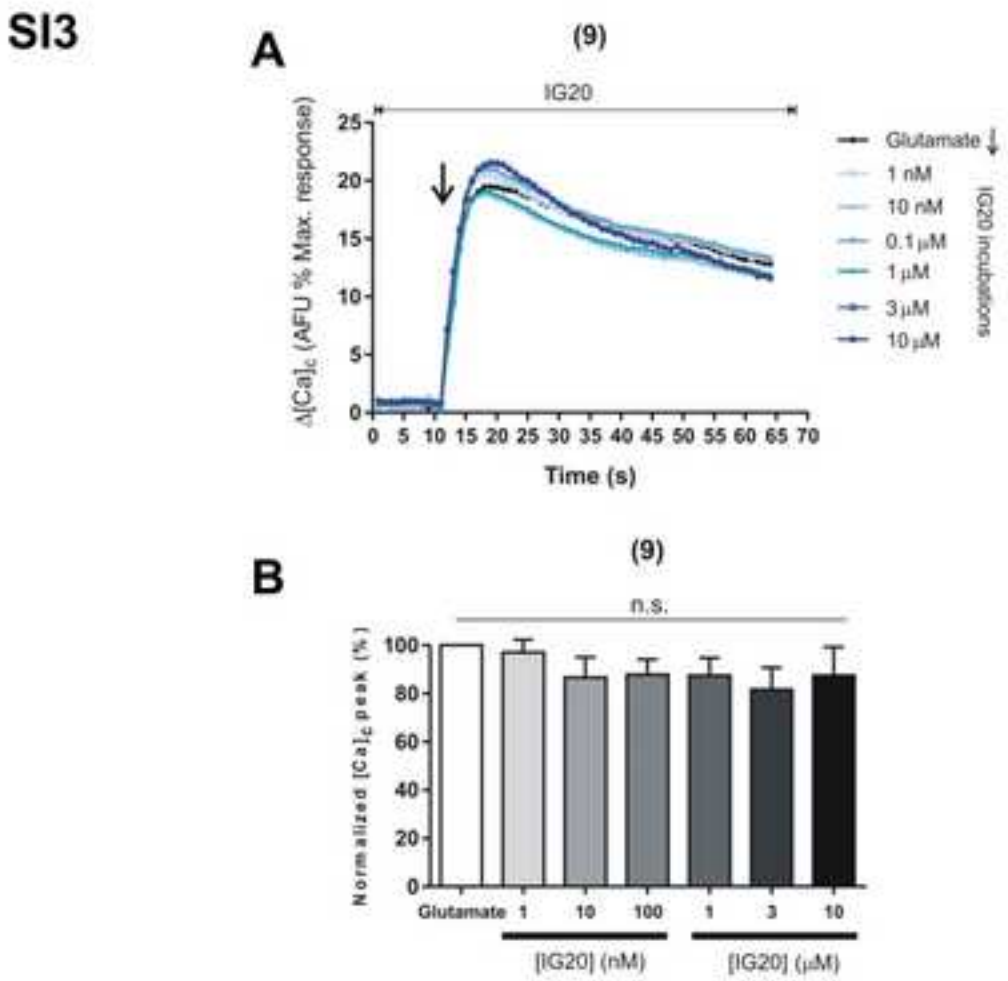

Supplementary Material

Click here to download Supplementary Material: Supporting Info-1(31-10-16).docx